Synthesis and interface characterization of CNTs on graphene

2017 Nanotechnology 28 054007

(http://iopscience.iop.org/0957-4484/28/5/054007)

IOP Publishing Nanotechnology
Nanotechnology 28 (2017) 054007 (10pp) doi:10.1088/1361-6528/28/5/054007

Synthesis and interface characterization of CNTs on graphene

Changjian Zhou[1], Richard Senegor[2], Zachary Baron[2], Yihan Chen[3], Salahuddin Raju[3], Anshul A Vyas[2], Mansun Chan[3], Yang Chai[4] and Cary Y Yang[2]

[1] School of Electronic and Information Engineering, South China University of Technology, Guangzhou 510640, People's Republic of China
[2] Center for Nanostructures, Santa Clara University, Santa Clara, CA 95053, USA
[3] Department of Electronic and Computer Engineering, Hong Kong University of Science and Technology, Hong Kong, People's Republic of China
[4] Department of Applied Physics, The Hong Kong Polytechnic University, Hong Kong, People's Republic of China

E-mail: zhoucj@scut.edu.cn

Received 24 October 2016, revised 16 November 2016
Accepted for publication 29 November 2016
Published 28 December 2016

Abstract

Carbon nanotubes (CNTs) and graphene are potential candidates for future interconnect materials. CNTs are promising on-chip via interconnect materials due to their readily formed vertical structures, their current-carrying capacity, which is much larger than existing on-chip interconnect materials such as copper and tungsten, and their demonstrated ability to grow in patterned vias with sub-50 nm widths; meanwhile, graphene is suitable for horizontal interconnects. However, they both present the challenge of having high-resistance contacts with other conductors. An all-carbon structure is proposed in this paper, which can be formed using the same chemical vapor deposition method for both CNTs and graphene. Vertically aligned CNTs are grown directly on graphene with an Fe or Ni catalyst. The structural characteristics of the graphene and the grown CNTs are analyzed using Raman spectroscopy and electron microscopy techniques. The CNT-graphene interface is studied in detail using transmission electron microscopic analysis of the CNT-graphene heterostructure, which suggests C−C bonding between the two materials. Electrical measurement results confirm the existence of both a lateral conduction path within graphene and a vertical conduction path in the CNT-graphene heterostructure, giving further support to the C−C bonding at the CNT-graphene interface and resulting in potential applications for all-carbon interconnects.

Keywords: interconnect, graphene, carbon nanotube, interface

(Some figures may appear in colour only in the online journal)

1. Introduction

To meet the stringent requirements of future integrated circuit (IC) interconnects for reduced signal delay and increased current-carrying capacity, various emerging materials and devices are being explored to replace existing mainstream copper and tungsten interconnects [1–7]. One of the primary challenges regarding copper interconnects with nanoscale linewidths is that the current density approaches or exceeds the current-carrying capacity $J_{max} \sim 2 \times 10^6$ A cm^{-2} due to electromigration [8, 9]. Carbon nanomaterials, with their promise of near-ballistic transport [10] and large current-carrying capacities, have been demonstrated as both horizontal interconnects (lines) [6, 11, 12] and vertical interconnects (vias) [13–17]. Both two-dimensional graphene and one-dimensional CNTs have been shown to exhibit current-carrying capacities which are orders of magnitude higher than that of copper [18–21]. Graphene would be an ideal candidate for horizontal interconnects due to its 2D geometry. Although work on the characterization of graphene as a horizontal

interconnect has been reported [6, 12], none of it has addressed the important issue of how graphene would fit into the overall on-chip interconnect network. Moreover, identifying and assessing suitable vertical via materials to be integrated with horizontal graphene interconnects is needed and requires in-depth studies of fabrication, interface analysis, and electrical characterization of the 3D test structure. On the other hand, vertically aligned CNTs have been readily obtained using various chemical vapor deposition (CVD) methods [22, 23], and CNT interconnect vias with widths down to 40 nm have been systematically studied [16, 21]. However, the CNT vias reported were grown on a metal underlayer, giving rise to significant contact resistance [13–17]. Thus it seems logical to explore a 3D all-carbon interconnect structure using vertical CNTs grown directly on the graphene [24–30].

In the characterizing J_{max} of CNTs, large values are obtained using individual CNTs with engineered contacts between them and the metal electrodes. Various contact engineering techniques [31], such as enhanced contact areas using a focused ion beam (FIB) prior to electrode formation [19] and Joule heating to form eutectic metal carbides at the contacts [20], have been used to ensure low-resistance contacts between the CNTs and the electrodes. However, for practical applications in integrated circuits (ICs), CNTs need to be grown at selected positions with areal densities approaching 10^{12} cm^2 to be competitive with copper and tungsten interconnects [17]. Thus the contact engineering techniques mentioned above for improving the performance of individual CNTs are not suitable for practical applications that require a large number of contacts to be processed. Graphene-based electronic devices also encounter similar contact resistance problems [32–34]. For on-chip applications, both horizontal and vertical interconnects are required to form a multi-level interconnect network. If only one form of carbon-based interconnect is used in conjunction with conventional metal interconnects, it is inevitable to include metal-carbon contacts on the chip. Although such contacts can be improved through careful metal choice and various post-treatment methods [31, 33, 35], integrating them into interconnect fabrication processes presents daunting challenges. Furthermore, even if these contact engineering techniques could be integrated into backend processes, the conventional metal lines/vias would pose the same problems in such hybrid nanocarbon-metal interconnect architecture, as linewidths continue to scale downwards.

In this paper, we present a study of an all-carbon interconnect structure using a 2D graphene horizontal network and vertically aligned CNTs as the vertical interconnect. The CNTs are directly grown on multi-layer graphene (MLG) to achieve C−C bonding at the interface. Ideally, if sp^2 bonding continues from the CNT into the graphene layer(s), the 3D structure should, in principle, yield low overall resistance as well as low contact resistance. Most recently, the electrical performance of an interconnect structure combining CNTs and graphene was demonstrated [24], but the corresponding structural and interface characteristics were not reported. A similar approach was also adopted for application in a through-silicon-via (TSV) for inter-chip interconnects [25]. Several reports have suggested that a CNT-graphene composite with graphene on top of vertical CNTs is obtainable through the optimization of growth parameters using Ni catalysts [36–38]. However, the graphene carpet on the CNTs forms an epitaxial interface with the CNT graphitic shells [37, 38], similar to the van der Waals bonding between adjacent layers of MLG. On the other hand, the growth of CNTs on graphene is reported to form a seamless 3D hybrid structure for electrochemical and energy storage applications [26–29, 39–41]. In fact, the CNT-graphene junction has been identified to show covalent bonding using transmission electron microscopic (TEM) analysis of the solvent-processed samples [28]. While the interface properties of CNT-graphene correlate with charge and heat transfer through the interface [42–45], the cross-section of a CNT-graphene interface has not been directly observed. As we report here, the CNT-graphene interface is thoroughly investigated using TEM analysis of the transferred CNT-graphene sample on a Cu grid and the prepared cross-section of the as-grown CNT/graphene on an oxide structure, revealing C−C bonding between the CNTs and the graphene. Electrical measurements of the CNT-graphene heterostructure confirm the existence of conduction paths in both lateral and vertical directions, which provide further evidence of continuous C−C bonding across the CNT-graphene interface. Successful demonstration of a conducting CNT-graphene structure can serve as the basis for further work on building a multi-level 3D all-carbon interconnect network.

2. Synthesis of CNT-graphene heterostructure

2.1. Fabrication process of CNT-graphene heterostructure

Fabrication of the CNT-graphene heterostructure consists of three steps: graphene growth on a substrate, graphene transfer onto a non-conductive substrate, and CNT growth on transferred graphene. Figure 1 shows the fabrication process flow and the CNT-graphene test structure. A fast microwave plasma-enhanced chemical vapor deposition (MPECVD) method is used to grow graphene using evaporated 300 nm thick Ni on a silicon substrate. The sample is first annealed at 900 °C in a H_2 atmosphere to increase the grain size of the Ni film and the uniformity of the graphene layer. This is followed by applying 200 W microwave power to ignite the plasma. Graphene growth is then initiated by introducing CH_4 as a carbon source. A typical recipe of H_2:CH_4 = 100 sccm:1 sccm at a pressure of 9.6 Torr is used. After ten seconds, the CH_4 gas flow is shut off and both the heater and plasma power are turned off to cool the substrate to room temperature in H_2 ambient. The growth mechanism consists of carbon dissociation, dissolving in Ni, and segregation on the Ni surface during the fast cooling process [46]. After growth, a 150 nm layer of PMMA is spin-coated on the graphene, which is then baked at 110 °C for 30 min to provide robust support in the subsequent releasing process. To enable graphene transfer onto other insulating substrates for further

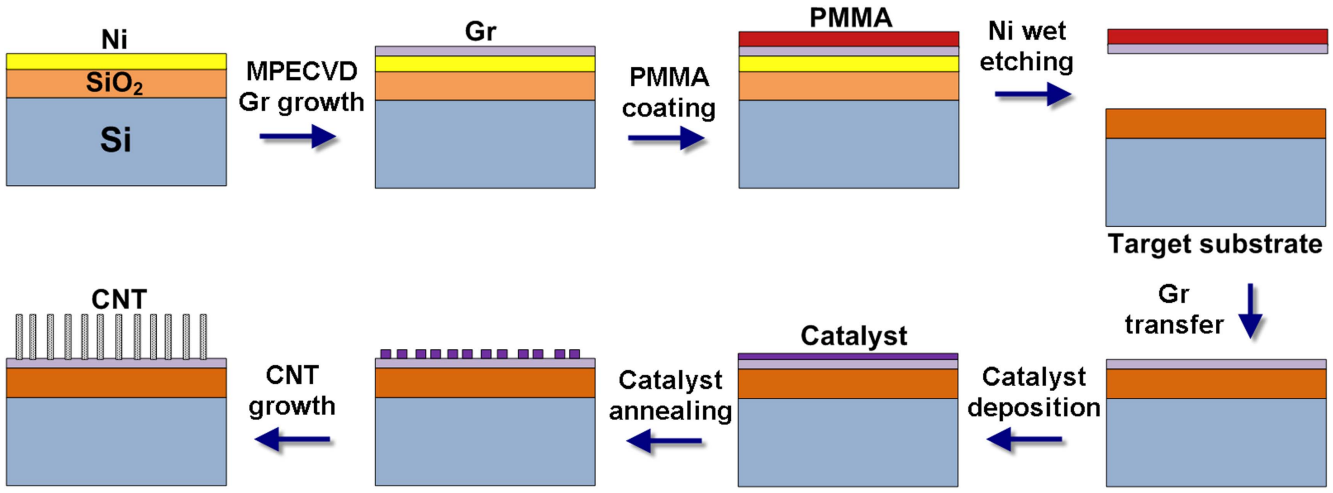

Figure 1. Process flow for CNT-graphene heterostructure fabrication.

electrical characterization and CNT growth, the PMMA-coated sample is put in a diluted HNO_3 solution. The Ni thin film underneath the graphene is etched by HNO_3 from the edges, leaving the PMMA-graphene film floating on the surface of the solution. The PMMA-graphene film is then transferred onto the target substrate and put on a hotplate. Any trapped water at the graphene-substrate interface is removed by slowly increasing the temperature of the hotplate to 90 °C. Then the PMMA is removed by rinsing the sample in acetone several times at 60 °C. A thin layer of metal catalyst—Fe or Ni—is deposited on the graphene by e-beam evaporation. Upon annealing, the metal thin film dewets to form nanoparticles. Finally, the CNTs are grown using the same MPECVD apparatus with CH_4 or C_2H_2 as the carbon source. The CNT-graphene heterostructure thus obtained is characterized using Raman spectroscopy, scanning electron microscopy (SEM) and TEM.

2.2. Growth of CNT on graphene

We have designed two sets of experiments for CNT growth using Fe and Ni catalysts, respectively, to study the catalyst dependence of CNT growth on graphene. For the first set, Fe is deposited by evaporation at a rate of 0.1 Å s^{-1}, resulting in a film thickness in the range of 2 Å $\sim$ 2 nm, to allow a study of the Fe film thickness dependence of CNT growth on graphene. The growth temperature is 850 °C, and the growth time is 1 min, with a ratio of CH_4:H_2:N_2 = 35 sccm:30 sccm:10 sccm at a pressure of 11 Torr and an applied plasma power of 200 W. For the second set of experiments, we used sputtered Ni ($\sim$1–2 nm) as the catalyst. The growth recipe is slightly different from the first set as we used C_2H_2 as the carbon source and a lower temperature of 700 °C. The growth process is similar to that for CNT vias [16, 21].

The as-grown CNT-graphene heterostructure was first examined using SEM. Figure 2 shows the cross-sectional SEM images of the CNTs grown using evaporated Fe film as the catalyst. Vertically aligned CNTs on graphene can be obtained using Fe film thicknesses in the range of 2 Å to 2 nm. The CNT growth rate is in the range of $\sim$2–13 μm min^{-1}, with the highest growth rate and best vertical alignment achieved when the catalyst film thickness is 5 Å. SEM analysis suggests that the graphene layer is preserved after CNT growth. Figure 3 shows that vertically aligned CNTs can also be grown on graphene using a Ni catalyst, with CNT diameters much wider than those grown with the Fe catalyst. For either case, further evidence is needed to confirm the existence of a true CNT-graphene heterostructure and the preservation of the graphene layer after CNT growth. Furthermore, the nanostructure at the CNT-graphene interface needs to be investigated. Thus extensive structural and interfacial characterizations have been conducted to address these questions, as detailed in the next section.

3. Structural and interface characterizations

3.1. Structural characterizations of graphene and CNTs

The structural characteristics of graphene and CNTs in the CNT-graphene heterostructure are investigated using Raman spectroscopy and TEM analysis. Figure 4 shows the optical microscope images and Raman spectra of the as-grown Ni-supported and transferred graphene samples. In the Raman spectra, the D band originates from the carbon rings consisting of sp^3-bonded carbon atoms at the defective sites or near edges, while the 2D band originates from a second-order process involving two phonons. The G band relates to the optical phonon mode between the two nonequivalent carbon atoms in the graphene unit cell, and is indicative of the presence of sp^2 C−C bonding [47]. The thickness of graphene grown on the Ni thin film is generally not uniform as carbon segregation at the final growth stage is dependent on the polycrystalline properties of the Ni film. The segregation rate at the grain boundary is usually faster than in the middle of a single grain, resulting in a thicker MLG near the boundary. This feature is clearly demonstrated in figure 4(b), where the SiO_2 substrate provides an ideal background to distinguish graphene layers with different thicknesses. The ratio of the 2D to G peak intensities serves as an indicator of the thickness of

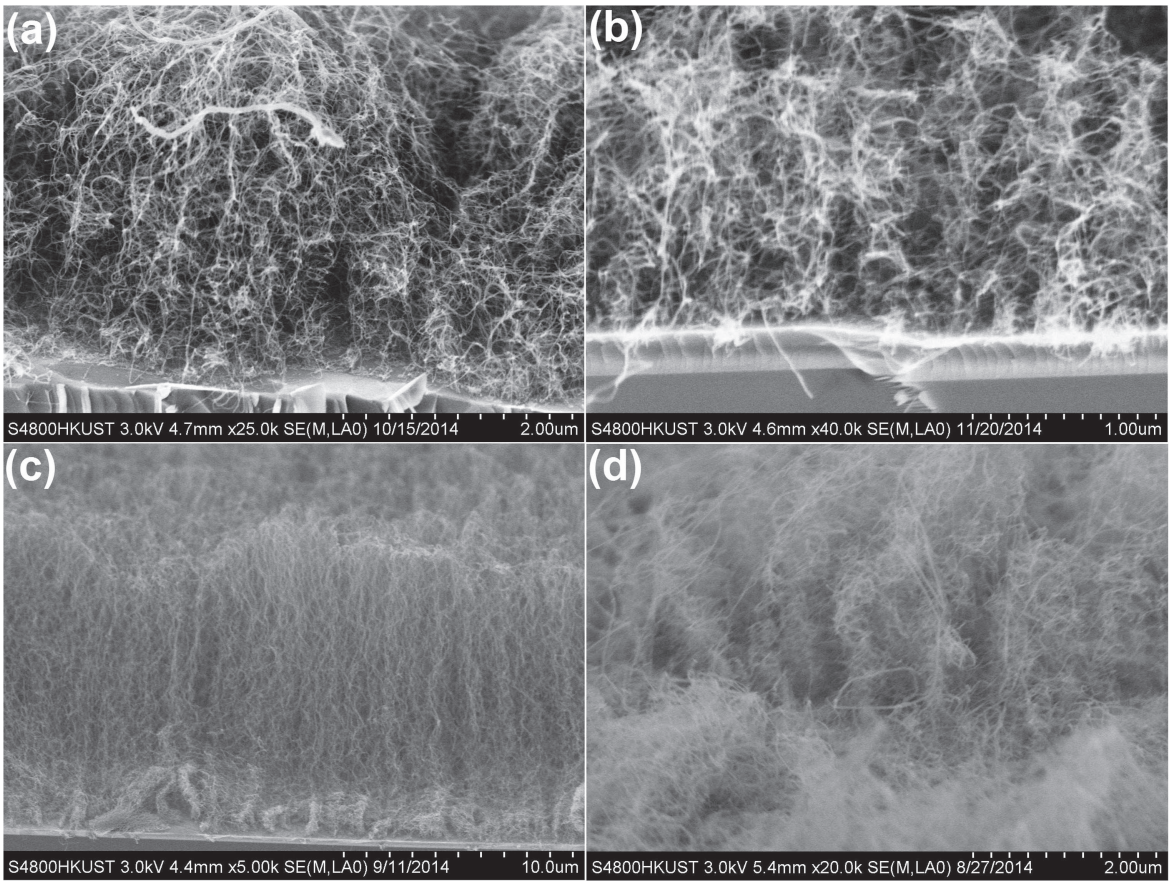

Figure 2. Cross-sectional SEM images of CNTs grown on graphene using Fe catalyst film with thicknesses of (a) 2 Å, (b) 3 Å, (c) 5 Å and (d) 1 nm.

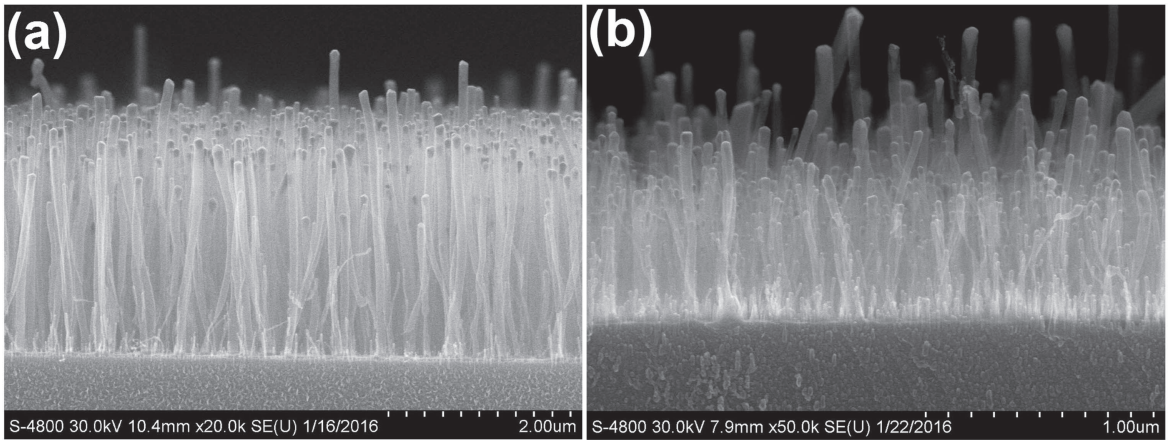

Figure 3. Cross-sectional SEM images of CNTs grown on graphene using Ni catalyst film with thicknesses of (a) ∼1 nm and (b) ∼1.5 nm.

the graphene [47]. The light purple area in figure 4(b) corresponds to $I_{2D}/I_G = 3.26$, which is typical for single-layer graphene. With the optimal growth parameters and a typical 10 s growth time, a large area of single-layer graphene can be obtained. The average thickness of the synthesized graphene is about three layers, estimated by comparing the optical transmittance of the graphene/quartz and the quartz substrate. We note that the graphene synthesized using this method is not usually uniform. For practical interconnect applications, multilayer graphene is needed to meet the low-resistance requirements, using two different approaches. Thicker multilayer graphene can be obtained with a longer growth time using the same method as in this work. Alternatively, it can be achieved by stacking transferred graphene layers multiple times.

The structure of CNTs grown on graphene is investigated using Raman spectroscopy. Since the laser spot covers an area occupied by many CNTs, multiple radial breathing modes (RBMs) are expected during each measurement. Each RBM peak corresponds to a specific CNT diameter. Figure 5 shows

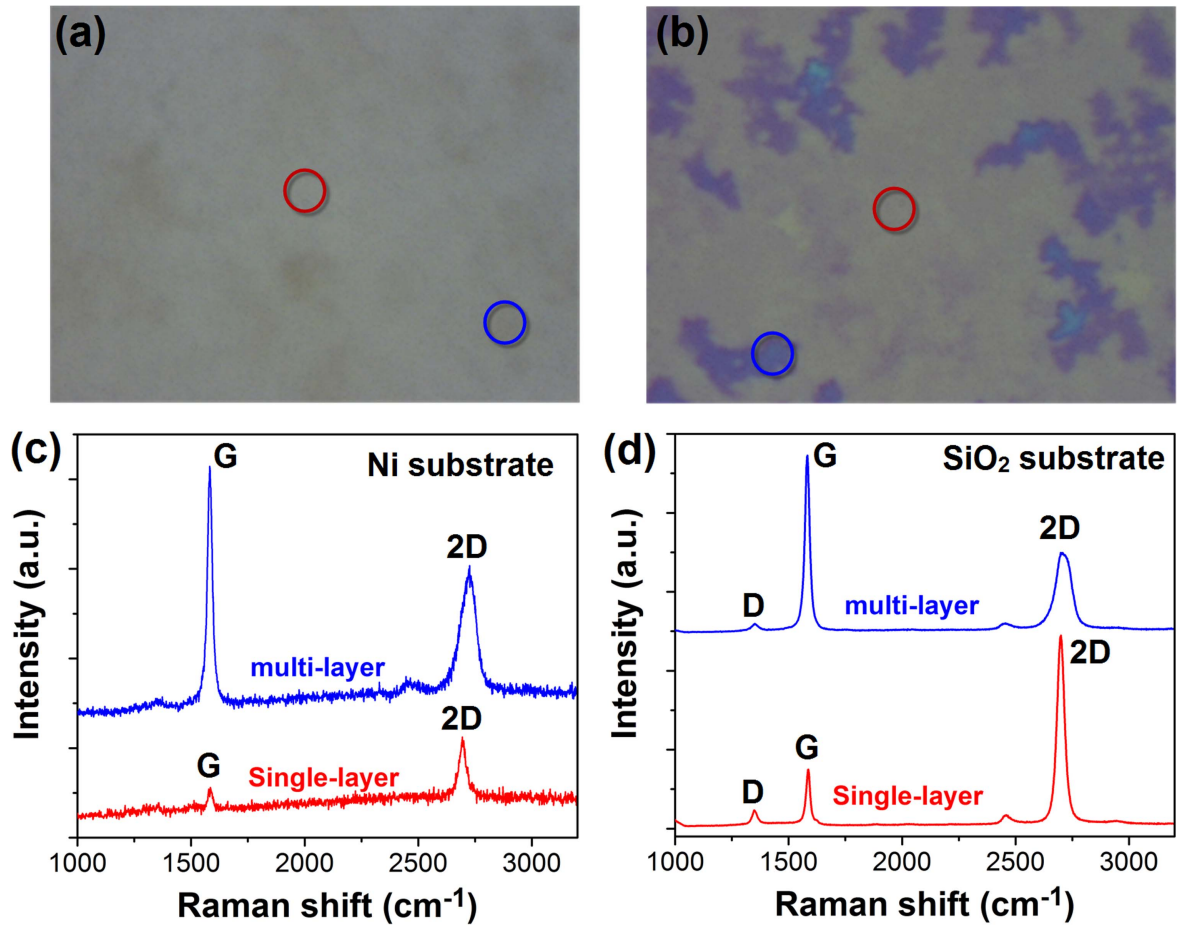

Figure 4. Optical microscope images of (a) as-grown graphene on the Ni substrate and (b) transferred graphene on the SiO_2 substrate; magnification 500×. The Raman spectra measured from graphene (c) on the Ni substrate and (d) transferred to the SiO_2 substrate; the circles in the optical images indicate the measured area corresponding to the results shown as red (single-layer graphene) and blue (multi-layer graphene) lines in (c) and (d). The excitation wavelength is 514 nm in the Raman experiments.

the Raman spectra of CNTs grown on graphene with the Fe catalyst. For all CNT samples, D, G and 2D bands are observed. The ratio of the D to G peak intensities, I_D/I_G, is a measure of the number of defect sites in the CNTs [48]. For the CNTs grown with a 1 nm Fe catalyst, $I_D/I_G = 1.20$ and decreases to 0.41 for CNTs grown with the 3 Å Fe catalyst. This indicates the improved CNT quality obtained with the thinner Fe film, as all other growth parameters, including the growth temperature, are kept the same for these experiments. The most striking difference among these Raman spectra is the appearance of single-walled CNTs (SWCNTs) with reduced Fe thickness. This is revealed by the RBM peaks at low frequencies, which only occur for SWCNTs [48], as indicated in the insets of figures 5(c) and (d). Figure 5(a) shows the highest I_D/I_G ratio among all the Raman spectra obtained. Relating this finding to the Fe catalyst thickness, the observed lower I_D/I_G ratio for CNTs grown with a thinner Fe catalyst is attributed to a lower percentage of multi-walled CNTs (MWCNTs). The RBM peaks shown in the insets of figures 5(c) and (d) lie in the 130–300 cm^{-1} range, corresponding to SWCNT diameters of 0.8 nm ∼ 1.9 nm [49]. In comparison, the CNTs grown with the Ni catalyst are mostly MWCNTs, and their Raman spectra resemble those of CNTs grown with a 1 nm Fe catalyst containing a relatively large number of defect sites [50].

3.2. Interface analysis of the CNT-graphene heterostructure

The key properties of the CNT-graphene heterostructure, such as mechanical strength, electrical conductance, and thermal conductance, are critically dependent on the interface between the CNT and graphene. We employ two methods for preparing the TEM samples for interface analysis. In the first method, the as-grown CNT-graphene heterostructure is directly transferred to a Cu grid for TEM analysis. While the as-grown CNTs on the graphene surface are no longer vertically aligned, but still attached to the graphene surface after the liquid-assisted transfer process, the original interface is preserved. In the second method, a cross-section of the CNT-graphene heterostructure is prepared using standard TEM sample preparation techniques, and both the graphene layer and the CNT-graphene interface remain intact for TEM imaging. This is the first report on such cross-sectional CNT-graphene interface images.

Figure 6(a) shows the TEM images of CNTs grown on graphene with the Fe catalyst using the first method. The inset in figure 6(a) shows the tip of one CNT with at least four

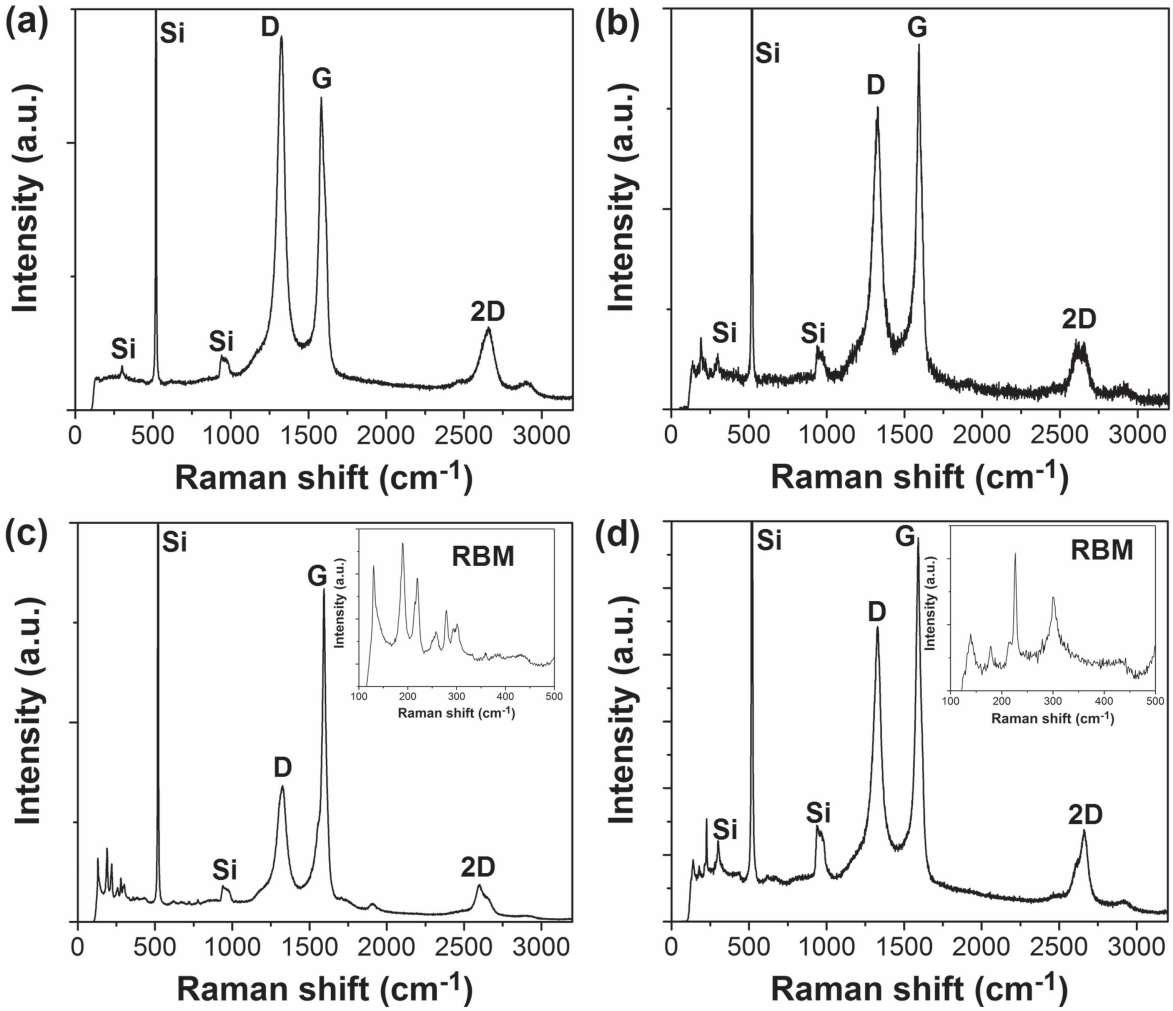

Figure 5. The Raman spectra of CNTs grown on graphene using Fe catalyst films with a thickness of (a) 1 nm, (b) 5 Å, (c) 3 Å and (d) 2 Å. The insets in (c) and (d) show the radial breathing modes (RBMs) of the SWCNTs. The three peaks at 301 cm^{-1}, 519 cm^{-1} and 940 cm^{-1} resulting from the silicon substrate are denoted as Si. The excitation wavelength is 633 nm.

graphitic walls (diameter 7.4 nm), encapsulating the Fe catalyst particle and confirming tip-growth for the CNT. To achieve a clean CNT-graphene interface, the tip-growth process is critical, and for these images, it also helps in locating the interface region between the CNT and the graphene, as shown in figure 6(b). At the interface, there are five to six rings (not all continuous) present on the graphene surface. Above these rings and along the length of the CNT, one can observe that these rings are connected to the CNT walls, which remain intact and extend through the graphene layers, strongly suggesting bonding between the carbon atoms from the CNT and graphene at the interface. Such interface bonding is further supported by the fact that the region of graphene in the immediate vicinity of the CNT-graphene interface remains intact, consistent with the notion of a seamless 3D CNT-graphene heterostructure. Similar results for another CNT with a diameter of 5.7 nm are presented in figure 6(c), which shows three walls of the CNT connected to the rings on the graphene surface.

We further examine the cross-section of the CNT-graphene heterostructure using the second method, which provides more information about the characteristics of the interface. Figure 7(a) shows a cross-sectional TEM image of the CNT-graphene heterostructure for the CNTs grown with the Fe catalyst. There are five to six graphene layers discernible on the oxide substrate, while the grown CNTs are encapsulated in the epoxy for protection during the preparation of the cross-section samples. Although the contrast between the CNT and epoxy is not very high, one can detect the presence of a CNT by locating the catalyst particle and the region of the distorted graphene, which lies underneath the CNT. The distorted graphene layers correspond to the rings observed in figures 6(b) and (c). Together with the TEM images of the directly transferred sample which shows rings on the graphene and CNT walls at the interface, these interfacial cross-sectional images strongly suggest that C−C bonding occurs between the atoms at the base of the CNT and those from the graphene layers. While we do not know at this time if such bonding is indeed sp^2, it is clear that unlike the contacts between the CNT or graphene and a conventional metal [31, 51, 52], which mostly exhibit van der Waals bonding, the CNT-graphene heterostructure can indeed yield continuous C−C bonding spanning the entire structure.

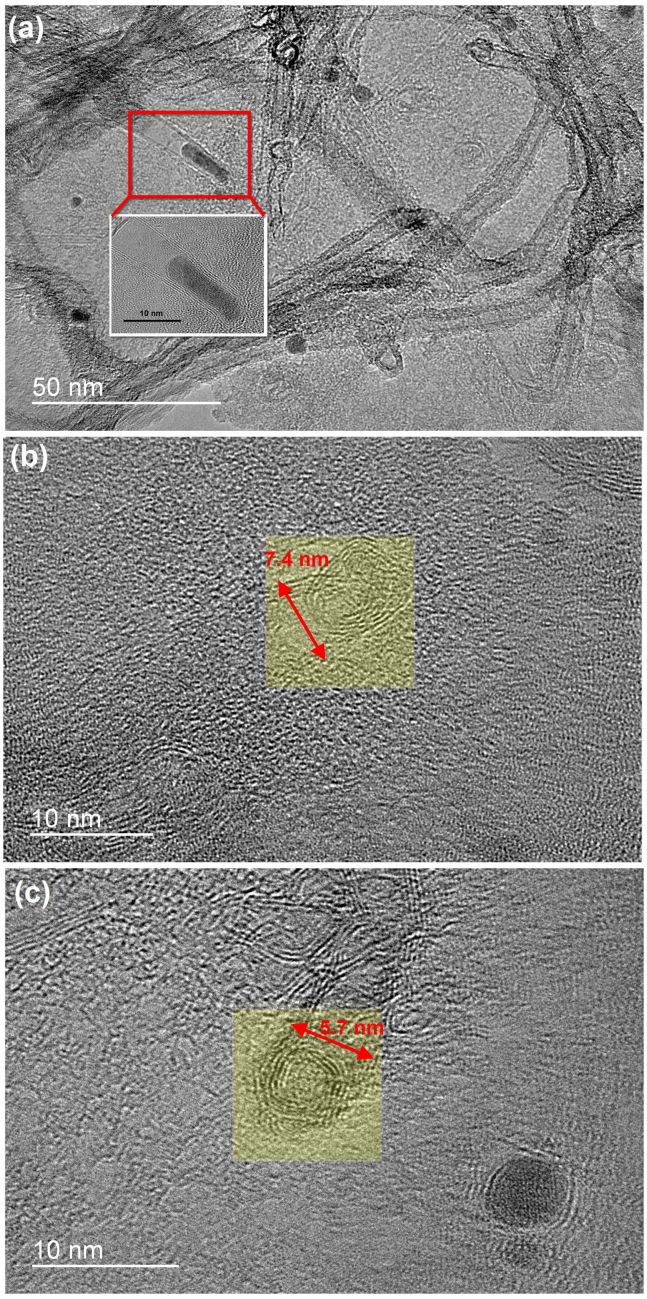

Figure 6. TEM images of the CNTs grown on graphene using the Fe catalyst. (a) The as-grown CNTs on the graphene transferred to a TEM copper grid; the inset shows the tip of a CNT with an Fe particle encapsulated by the CNT walls. (b), (c) The interface regions between the CNT and the graphene; the yellow highlighted area shows the rings formed on the graphene and the interface between the CNT and the graphene.

In view of the extensive use of Ni as a catalyst for CNT growth, it is of interest to compare the results of CNTs grown on graphene with Ni to those with Fe. Figure 7(b) shows a cross-sectional TEM image of the CNT-graphene interface for CNTs grown with the Ni catalyst. First, some graphene layers are missing, especially in the regions where CNT growth takes place. This is attributed to etching of the graphene by Ni. This etching phenomenon has also been discovered by other researchers in exploring Ni etching effects and the

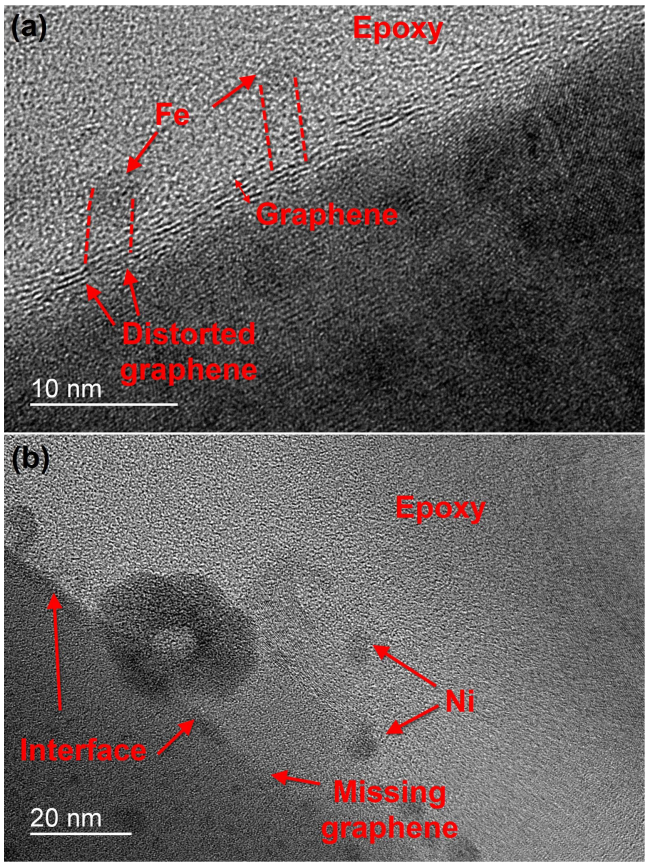

Figure 7. Cross-sectional TEM images of the CNTs grown on graphene with (a) the Fe catalyst and (b) the Ni catalyst. Distorted graphene is indicated near the base of the grown CNT in (a), while some graphene is missing at the interface after the CNT growth in (b).

formation of graphene nanoribbons [53, 54]. It was also reported that the graphene dissolved in Ni could be a source for CNT growth [30], which is verified in our own experiments where CNT growth takes place on Ni-coated graphene, even without any additional carbon sources. The difference in the nanostructure interface between the CNTs and graphene obtained with the two different catalysts suggests that the Fe catalyst is more suitable for preserving graphene and achieving C−C bonding across the CNT-graphene interface.

3.3. Electrical characteristics of CNT-graphene heterostructure

In this section, the electrical characteristics of the CNT-graphene heterostructure based on two-terminal current–voltage (I–V) measurements are presented. The results provide evidence that the CNT-graphene heterostructure exhibits electrical conduction paths, which are not disrupted by the CNT growth process. First, the electrical characteristics of the graphene layer after CNT growth are measured to determine the sheet resistance and contact resistance between the electrical probes and the graphene. The graphene layers are patterned into strips 20 μm wide with varying lengths from 10–100 μm. As shown in figure 8(a), the measurements yield a sheet resistance of 1821 $\Omega\ \square^{-1}$ and a contact resistivity of 950 $\Omega \cdot \mu$m, consistent with the values obtained for pristine

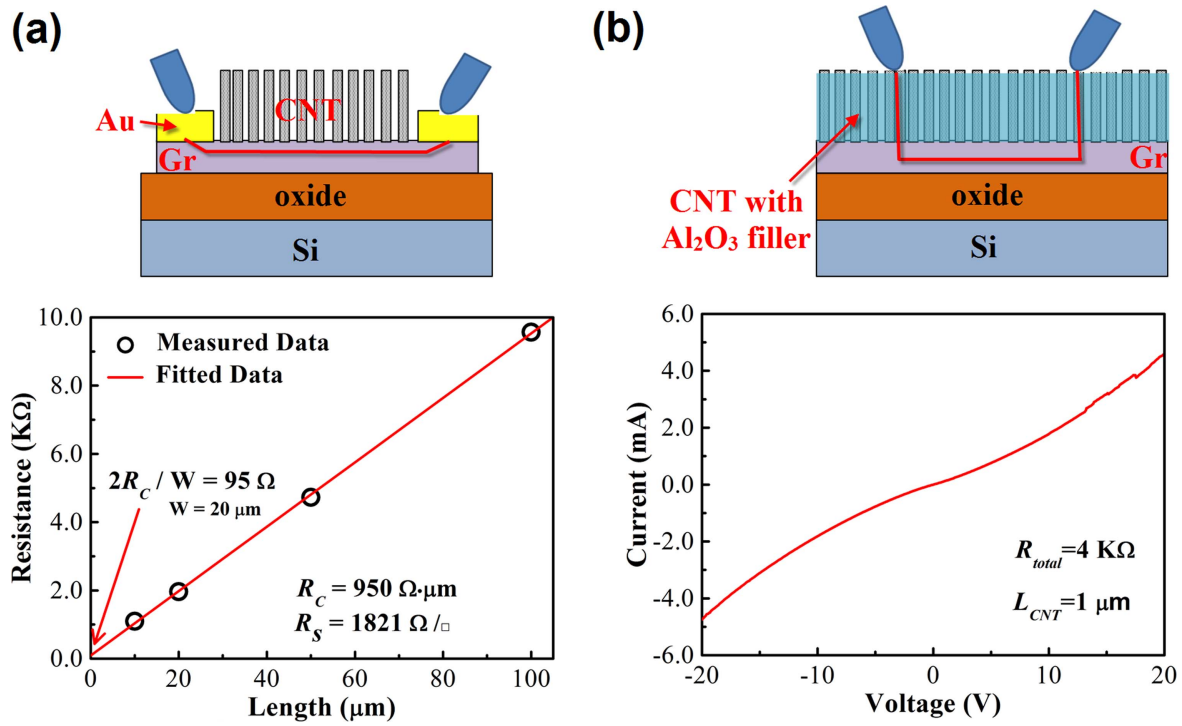

Figure 8. (a) A schematic of the electrical measurement and resistance versus graphene length behavior after CNT growth, where W denotes the width of the graphene strip, R_S the sheet resistance, and R_C the contact resistivity. (b) A schematic of the electrical measurement and I–V characteristics of the CNT-graphene heterostructure after oxide filling and polishing to expose the CNT tips, where R_{total} denotes the total extracted resistance and L_{CNT} the CNT height.

graphene on oxide substrates [55]. Thus the CNT growth process, which consists of Fe film deposition, annealing, and CNT growth using PECVD, does not seem to be detrimental to the graphene layers. The results also confirm the existence of a lateral conduction path in graphene. One advantage of using graphene as a lateral interconnect is its large current-carrying capacity. It has been reported that CVD graphene has a J_{max} up to 4×10^7 A cm^{-2} [18]. We performed the I–V measurements of graphene samples after CNT growth. The measurement setup is the same as in the schematic of figure 8(a). An increasing voltage is applied to the graphene strips until breakdown occurs, when the J_{max} is extracted to yield 4.32×10^7 A cm^{-2} and 7.43×10^7 A cm^{-2} for the two graphene samples with 10 μm and 20 μm channel widths, respectively. Thus the results confirm that the graphene layer preserves its large current-carrying capacity after the CNT growth process.

After CNT growth, an oxide layer prepared by the atomic layer deposition (ALD) method is used to fill the voids between the CNTs. Then, carefully controlled rinsing in buffered hydrogen fluoride is carried out to remove the oxide from the top of the CNT, leaving the tips of the CNTs exposed for direct probing, as shown in the measurement schematic in figure 8(b). The measured I–V behavior is nonlinear, suggesting non-ohmic transport across the probe-CNT contacts and/or CNT-graphene interface. Nevertheless, the extracted total resistance of ~4 kΩ for the CNT-graphene heterostructure does indicate the existence of conduction paths throughout the 3D structure. Using the results from figure 8(a), each graphene strip contributes ~3 kΩ to the total resistance. The CNT resistance, which can be assumed to originate from two CNT vias 1 μm high with a cross-sectional area of 2 μm × 2 μm (the tip area of the probe), estimated using the data obtained from sub-100 nm CNT vias [21], is no more than 100 Ω. The remaining resistance mainly comes from the contacts. The total resistance decreases as the applied voltage increases, due to the improved contact from the Joule heating during the measurement, a well-known phenomenon for CNT-metal contacts [31]. Further experiments, such as *in situ* nanoprobing of the individual CNTs inside an SEM chamber, are needed to extract the contact resistance of the CNT-graphene interface. Nevertheless, these electrical measurements have demonstrated the existence of both vertical and lateral conduction paths in the CNT-graphene heterostructure, and they provide independent support for the viability of a 3D CNT-graphene interconnect network.

4. Summary

The direct integration of CNTs with graphene to form a 3D CNT-graphene heterostructure is experimentally investigated using Fe and Ni catalysts. Both the graphene and CNTs are synthesized using the same CVD method with different recipes. With the Fe catalyst, SWCNTs can be obtained when the Fe film thickness is reduced to 5 Å or below, while mostly MWCNTs result with thicker Fe or Ni film. We have analyzed the interface between the CNTs and graphene using two TEM sample preparation methods. At the CNT-graphene interface, there are several rings surrounding the grown CNTs

connected to the CNT walls that extend through the graphene layers. The cross-sectional TEM images confirm that the CNT protrudes from the graphene layers, distorting the layers underneath it. These observations, supported by electrical measurements, strongly suggest some form of C−C bonding between the carbon atoms at the CNT-graphene interface for the CNTs grown with the Fe catalyst. In comparison, the CNTs grown with the Ni catalyst tend to result in severe damage to the graphene layers due to the etching effect of the Ni. These findings will pave the way for further studies on 3D all-carbon interconnects.

Acknowledgments

This work was supported by the Research Grant Council of Hong Kong (grant no. PolyU 252001/14E, 16203851, and AOE/P-04/08-1), together with the Hong Kong Polytechnic University (grant no. H-ZG1N and 1-ZE25). We acknowledge the Nanosystem Fabrication Facility (NFF) of HKUST for device fabrication and the collaborative Research Fund C6007-15E from RGC for providing the laser direct write machine to make this work possible.

References

[1] Behin-Aein B, Datta D, Salahuddin S and Datta S 2010 Proposal for an all-spin logic device with built-in memory *Nat. Nanotechnol.* **5** 266–70
[2] Kincal S, Abraham M C and Schuegraf K 2014 RC performance evaluation of interconnect architecture options beyond the 10 nm logic node *IEEE Trans. Electron Devices* **61** 1914–9
[3] Adelmann C, Wen L G, Peter A P, Siew Y K, Croes K, Swerts J, Popovici M, Sankaran K, Pourtois G and Van Elshocht S 2014 Alternative metals for advanced interconnects *IEEE Int. Interconnect Technology Conf./ Advanced Metallization Conf. (IITC/AMC) (San Jose, CA, 2014)* pp 173–6
[4] Kreupl F, Graham A P, Duesberg G, Steinhögl W, Liebau M, Unger E and Hönlein W 2002 Carbon nanotubes in interconnect applications *Microelectron. Eng.* **64** 399–408
[5] Li B, Luo Z, Shi L, Zhou J, Rabenberg L, Ho P S, Allen R A and Cresswell M W 2009 Controlled formation and resistivity scaling of nickel silicide nanolines *Nanotechnology* **20** 085304
[6] Murali R, Brenner K, Yang Y, Beck T and Meindl J D 2009 Resistivity of graphene nanoribbon interconnects *IEEE Electron Device Lett.* **30** 611–3
[7] Sankaran K, Clima S, Mees M and Pourtois G 2015 Exploring alternative metals to Cu and W for interconnects applications using automated first-principles simulations *ECS J. Solid State Sci. Technol.* **4** N3127–33
[8] Li B, Christiansen C, Badami D and Yang C-C 2014 Electromigration challenges for advanced on-chip Cu interconnects *Microelectron. Reliab.* **54** 712–24
[9] Chai Y, Chan P C, Fu Y, Chuang Y and Liu C 2008 Electromigration studies of Cu/carbon nanotube composite interconnects using Blech structure *IEEE Electron Device Lett.* **29** 1001–3
[10] Li H J, Lu W G, Li J J, Bai X D and Gu C Z 2005 Multichannel ballistic transport in multiwall carbon nanotubes *Phys. Rev. Lett.* **95** 086601
[11] Chen X, Lee K-J, Akinwande D, Close G F, Yasuda S, Paul B, Fujita S, Jing Kong S and Wong H-S P 2009 High-speed graphene interconnects monolithically integrated with CMOS ring oscillators operating at 1.3 GHz *IEEE Int. Electron Devices Meeting (IEDM) (Baltimore, MD)* pp 581–4
[12] Yu T, Liang C-W, Kim C, Song E-S and Yu B 2011 Three-dimensional stacked multilayer graphene interconnects *IEEE Electron Device Lett.* **32** 1110–2
[13] Ngo Q, Cassell A M, Austin A J, Li J, Krishnan S, Meyyappan M and Yang C Y 2006 Characteristics of aligned carbon nanofibers for interconnect via applications *IEEE Electron Device Lett.* **27** 221–4
[14] Coiffic J, Fayolle M, Le Poche H, Maitrejean S and Olivier S 2008 Realization of via interconnects based on carbon nanotubes *IEEE Int. Intercconnect Technology Conf. (Burlingame, CA)* pp 153–5
[15] Vollebregt S, Chiaramonti A N, van der Cingel J, Beenakker K and Ishihara R 2013 Towards the integration of carbon nanotubes as vias in monolithic three-dimensional integrated circuits *Japan. J. Appl. Phys.* **52** 04CB2
[16] Zhou C, Vyas A A, Wilhite P, Wang P, Chan M and Yang C Y 2015 Resistance determination for sub-100 nm carbon nanotube vias *IEEE Electron Device Lett.* **36** 71–3
[17] Nihei M, Kawabata A, Kondo D, Horibe M, Sato S and Awano Y 2005 Electrical properties of carbon nanotube bundles for future via interconnects *Japan. J. Appl. Phys.* **44** 1626–8
[18] Lee K-J, Chandrakasan A P and Kong J 2011 Breakdown current density of CVD-grown multilayer graphene interconnects *IEEE Electron Device Lett.* **32** 557–9
[19] Wei B Q, Vajtai R and Ajayan P M 2001 Reliability and current carrying capacity of carbon nanotubes *Appl. Phys. Lett.* **79** 1172
[20] Santini C A, Vereecken P M, Volodin A, Groeseneken G, De Gendt S and Haesendonck C V 2011 A study of Joule heating-induced breakdown of carbon nanotube interconnects *Nanotechnology* **22** 395202
[21] Vyas A A, Zhou C, Chai Y, Wang P and Yang C Y 2016 Effect of improved contact on reliability of sub-60 nm carbon nanotube vias *Nanotechnology* **27** 375202
[22] Nozaki T, Ohnishi K, Okazaki K and Kortshagen U 2007 Fabrication of vertically aligned single-walled carbon nanotubes in atmospheric pressure non-thermal plasma CVD *Carbon* **45** 364–74
[23] Chhowalla M, Teo K B K, Ducati C, Rupesinghe N L, Amaratunga G A J, Ferrari A C, Roy D, Robertson J and Milne W I 2001 Growth process conditions of vertically aligned carbon nanotubes using plasma enhanced chemical vapor deposition *J. Appl. Phys.* **90** 5308
[24] Ramos R F A, Fayolle M, Dijon J, Murray C P and McKenna J 2016 Nano carbon interconnects combining vertical CNT interconnects and horizontal graphene lines *IEEE Int. Interconnect Technology Conf./Advanced Metallization Conf. (IITC/AMC) (San Jose, CA)* pp 48–50
[25] Ghosh K, Ranjan N, Verma Y K and Tan C S 2016 Graphene–CNT hetero-structure for next generation interconnects *RSC Adv.* **6** 53054–61
[26] Ryu J-H, Lee G-J, Kim W-S, Lim H-E, Mativenga M, Park K-C and Park H-K 2014 All-carbon electrode consisting of carbon nanotubes on graphite foil for flexible electrochemical applications *Materials* **7** 1975–83
[27] Rao R, Chen G, Arava L M, Kalaga K, Ishigami M, Heinz T F, Ajayan P M and Harutyunyan A R 2013 Graphene as an atomically thin interface for growth of vertically aligned carbon nanotubes *Sci. Rep.* **3** 1891

[28] Zhu Y *et al* 2012 A seamless three-dimensional carbon nanotube graphene hybrid material *Nat. Commun.* **3** 1225
[29] Lee D H, Kim J E, Han T H, Hwang J W, Jeon S, Choi S Y, Hong S H, Lee W J, Ruoff R S and Kim S O 2010 Versatile carbon hybrid films composed of vertical carbon nanotubes grown on mechanically compliant graphene films *Adv. Mater.* **22** 1247–52
[30] Kim Y S, Kumar K, Fisher F T and Yang E H 2012 Out-of-plane growth of CNTs on graphene for supercapacitor applications *Nanotechnology* **23** 015301
[31] Wilhite P, Vyas A A, Tan J, Tan J, Yamada T, Wang P, Park J and Yang C Y 2014 Metal–nanocarbon contacts *Semicond. Sci. Technol.* **29** 054006
[32] Nagashio K, Nishimura T, Kita K and Toriumi A 2010 Contact resistivity and current flow path at metal/graphene contact *Appl. Phys. Lett.* **97** 143514
[33] Xia F, Perebeinos V, Lin Y M, Wu Y and Avouris P 2011 The origins and limits of metal-graphene junction resistance *Nat. Nanotechnol.* **6** 179–84
[34] Venugopal A, Colombo L and Vogel E M 2010 Contact resistance in few and multilayer graphene devices *Appl. Phys. Lett.* **96** 013512
[35] Song S M, Park J K, Sul O J and Cho B J 2012 Determination of work function of graphene under a metal electrode and its role in contact resistance *Nano Lett.* **12** 3887–92
[36] Choi J W, Youn S K and Park H G 2013 Carbon micronymphaea: graphene on vertically aligned carbon nanotubes *J. Nanomater.* **2013** 1–7
[37] Jousseaume V, Cuzzocrea J, Bernier N and Renard V T 2011 Few graphene layers/carbon nanotube composites grown at complementary-metal-oxide-semiconductor compatible temperature *Appl. Phys. Lett.* **98** 123103
[38] Kondo D, Sato S and Awano Y 2008 Self-organization of novel carbon composite structure: graphene multi-layers combined perpendicularly with aligned carbon nanotubes *Appl. Phys. Express* **1** 074003
[39] Yang Z Y, Zhao Y F, Xiao Q Q, Zhang Y X, Jing L, Yan Y M and Sun K N 2014 Controllable growth of CNTs on graphene as high-performance electrode material for supercapacitors *ACS Appl. Mater. Interfaces* **6** 8497–504
[40] Yan Z *et al* 2014 Rebar graphene *ACS Nano* **8** 5061–8
[41] Yan Z *et al* 2013 Three-dimensional metal-graphene-nanotube multifunctional hybrid materials *ACS Nano* **7** 58–64
[42] Chen J, Walther J H and Koumoutsakos P 2015 Covalently bonded graphene-carbon nanotube hybrid for high-performance thermal interfaces *Adv. Funct. Mater.* **25** 7539–45
[43] Shi J, Dong Y, Fisher T and Ruan X 2015 Thermal transport across carbon nanotube-graphene covalent and van der Waals junctions *J. Appl. Phys.* **118** 044302
[44] Novaes F D, Rurali R and Ordejon P 2010 Electronic transport between graphene layers covalently connected by carbon nanotubes *ACS Nano* **4** 7596–602
[45] Varshney V, Patnaik S S, Roy A K, Froudakis G and Farmer B L 2010 Modeling of thermal transport in pillared-graphene architectures *ACS Nano* **4** 1153–61
[46] Yu Q, Lian J, Siriponglert S, Li H, Chen Y P and Pei S-S 2008 Graphene segregated on Ni surfaces and transferred to insulators *Appl. Phys. Lett.* **93** 113103
[47] Malard L M, Pimenta M A, Dresselhaus G and Dresselhaus M S 2009 Raman spectroscopy in graphene *Phys. Rep.* **473** 51–87
[48] Dresselhaus M S, Dresselhaus G, Saito R and Jorio A 2005 Raman spectroscopy of carbon nanotubes *Phys. Rep.* **409** 47–99
[49] Jorio A, Saito R, Hafner J H, Lieber C M, Hunter M, McClure T, Dresselhaus G and Dresselhaus M S 2001 Structural (n, m) determination of isolated single-wall carbon nanotubes by resonant Raman scattering *Phys. Rev. Lett.* **86** 1118–21
[50] Vyas A A, Zhou C, Wilhite P, Wang P and Yang C Y 2016 Electrical properties of carbon nanotube via interconnects for 30 nm linewidth and beyond *Microelectron. Reliab.* **61** 35–42
[51] Matsuda Y, Deng W-Q and Goddard W A 2007 Contact resistance properties between nanotubes and various metals from quantum mechanics *J. Phys. Chem.* C **111** 11113–6
[52] Matsuda Y, Deng W-Q and Goddard W A 2010 Contact resistance for 'end-contacted' metal−graphene and metal −nanotube interfaces from quantum mechanics *J. Phys. Chem.* C **114** 17845–50
[53] Campos L C, Manfrinato V R, Sanchez-Yamagishi J D, Kong J and Jarillo-Herrero P 2009 Anisotropic etching and nanoribbon formation in single-layer graphene *Nano Lett.* **9** 2600–4
[54] Kumar K, Kim Y-S, Li X, Ding J, Fisher F T and Yang E-H 2013 Chemical vapor deposition of carbon nanotubes on monolayer graphene substrates: reduced etching via suppressed catalytic hydrogenation using C_2H_4 *Chem. Mater.* **25** 3874–9
[55] Park H J, Meyer J, Roth S and Skákalová V 2010 Growth and properties of few-layer graphene prepared by chemical vapor deposition *Carbon* **48** 1088–94